

Evolution of valence-specific spin states and local distortions in $\text{La}_{2-x}\text{Sr}_x\text{CoO}_4$

J. Okamoto,^{1,*} A. Chainani,¹ Z. Y. Chen,² H. Y. Huang,¹ A. Singh,¹ T. Sasagawa,³ D. I. Khomskii,⁴ A. Fujimori,⁵ C. T. Chen,¹ and D. J. Huang^{1,2,†}

¹*National Synchrotron Radiation Research Center, Hsinchu 30076, Taiwan*

²*Department of Physics, National Tsing Hua University, Hsinchu 30013, Taiwan*

³*Materials and Structures Laboratory, Tokyo Institute of Technology, Yokohama, Kanagawa 226-8503, Japan*

⁴*II. Physikalisches Institut, Universität zu Köln, Zùlpicher Straße 77, D-50937 Köln, Germany*

⁵*Department of Applied Physics, Waseda University, Tokyo 169-8555, Japan*

(Dated: October 22, 2021)

We present X-ray spectroscopic evidence for the evolution of valence-specific spin states and tetragonal distortions in single-layer cobaltates. Measurements of Co L_3 -edge resonant inelastic X-ray scattering reveal the t_{2g} electronic structure of Co for hole-doped $\text{La}_{2-x}\text{Sr}_x\text{CoO}_4$ ($x = 0.5, 0.7$ and 0.8). As the Sr-doping x increases, the tetragonal splitting of the t_{2g} states of high-spin Co^{2+} decreases, whereas that of low-spin Co^{3+} increases and the fraction of high-spin Co^{3+} increases. The results enable us to clarify the origin of the change of magnetic anisotropy and in-plane resistivity in a mixed-valence cobaltate caused by the interplay of spin-orbit coupling and tetragonal distortion.

PACS numbers: 75.30.Wx, 71.70.Ch, 78.70.En

In strongly correlated $3d$ -transition-metal oxides, orderings of charge, spin and orbital degrees of freedom compete and cooperate with each other through coupling with the lattice [1, 2]. In particular, the orbital degeneracy and its lifting due to an external lattice distortion or a Jahn-Teller (JT) effect leads to various electronic or lattice instabilities. For instance, perovskite manganites exhibit various spin structures and complicated phase diagram arising from the orbital degree of freedom [3–5]. In addition, the spin-orbit coupling in compounds in which the t_{2g} orbitals are partially filled gives rise to a specific change in magnetic anisotropy as the distortions caused by the JT effect have effect typically opposite to those due to the spin-orbit interaction [6–8]. Doping holes into a K_2NiF_4 -type antiferromagnetic Mott insulator typically leads to novel phases, the most striking example being high-transition-temperature superconductors [2, 9, 10]. Single-layer perovskite “214” cobaltates $\text{La}_{2-x}\text{Sr}_x\text{CoO}_4$ are also K_2NiF_4 -type hole-doped Mott insulators and have attracted much attention because they share unusual physical properties with cuprates: checkerboard-type charge ordering [11–13], hourglass-shaped spin excitations [14–17] and nanoscale-phase separation [12, 17–19]. Apart from the general features common for many 214 systems, the cobaltates have yet very specific properties due to the existence of several competing spin states of Co^{3+} —magnetic high spin (HS) and non-magnetic low spin (LS) states, as discussed below. This makes the behaviour of these systems even richer.

The crystal structure of these layered cobaltates is illustrated in Fig. 1(a). The competition between crystal-field splitting $10Dq$ and intra-atomic Hund’s exchange interaction J_H dictates the spin state of Co ions in $\text{La}_{2-x}\text{Sr}_x\text{CoO}_4$ [20, 21]. Figure 1(b) shows the electronic energy levels of Co^{2+} and Co^{3+} under the D_{4h} crystal field according to a one-electron picture. The e_g and t_{2g}

states of Co $3d$ are further split by the tetragonal lattice distortion typical for all layered systems of 214 type; these splittings are denoted Δ_{e_g} and $\Delta_{t_{2g}}$, respectively. For a HS Co^{2+} or Co^{3+} ion, the JT distortion yields an additional contribution to the t_{2g} splitting.

$\text{La}_{2-x}\text{Sr}_x\text{CoO}_4$ is a strong insulator for all Sr doping concentrations; at half doping, $x = 0.5$, it possesses the largest resistivity [23] because of checkerboard-type charge ordering of Co^{2+} and Co^{3+} , leading to the spin blockade [24, 25]. In addition, the system exhibits pronounced magnetic anisotropy arising from band structure and spin-orbit coupling [7]. Various experimental techniques including neutron scattering [11–13, 26–28], magnetic susceptibility [7, 23, 29] and X-ray absorption spectroscopy (XAS) [25] have been applied to study the electronic structures that underlie the phase diagram of $\text{La}_{2-x}\text{Sr}_x\text{CoO}_4$. The elucidation of the change of the spin-state and electronic properties of Co^{2+} and Co^{3+} ions in response to the change of hole doping remains, however, a challenging task. To clarify this question is the main goal of the present investigation.

Resonant inelastic X-ray scattering (RIXS) is an effective spectroscopic method to measure excitations of correlated-electron materials derived from charge, spin, orbital and lattice degrees of freedom [30]. A series of Co L_3 -edge RIXS measurements recently enabled the unraveling of the valence and spin states of Co oxides in relation to their physical properties [21, 31–35]. Here we present Co L_3 -edge RIXS of $\text{La}_{2-x}\text{Sr}_x\text{CoO}_4$ to investigate the Co spin states and the tetragonal distortion by comparing the measured RIXS spectra with the cluster-model calculations. The results indicate that the tetragonal distortion of Co^{3+}O_6 and the HS population of Co^{3+} increase with increased Sr doping, whereas those of Co^{2+}O_6 decrease. Concomitant change of the spin state of Co^{3+} is also observed.

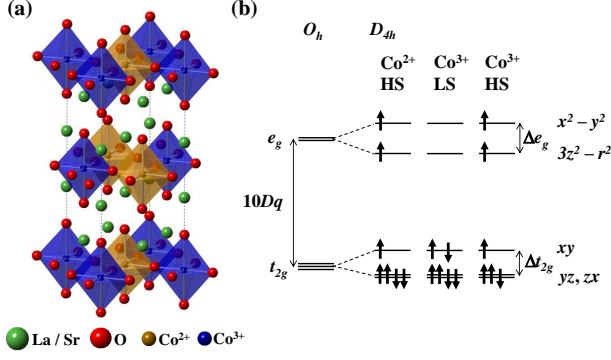


FIG. 1: (a) K_2NiF_4 -type lattice structure of $La_{1.5}Sr_{0.5}CoO_4$ with a checkerboard-type charge ordering. (b) Illustration of the energy levels of Co 3d states in a tetragonal D_{4h} crystal field with a CoO_6 octahedron elongated along the c -axis for HS Co^{2+} , LS and HS Co^{3+} . These levels are presented in a one-electron picture excluding the spin-orbit interaction. The tetragonal splittings can be expressed as $\Delta_{e_g} = 4D_s + 5D_t$ and $\Delta_{t_{2g}} = 3D_s - 5D_t$ in terms of parameters D_s and D_t according to the Ballhausen notation [22].

Single crystals of $La_{2-x}Sr_xCoO_4$ were grown by the floating-zone method [36]. The crystals were cut and polished for $x = 0.5$ or naturally cleaved for $x = 0.7$ and 0.8 with the sample surface in the ab plane. We recorded Co $L_{2,3}$ -edge XAS using the partial-fluorescence-yield method at Taiwan Light Source (TLS) beamline 08B of National Synchrotron Radiation Research Center (NSRRC) in Taiwan. The XAS energy resolution was ~ 0.3 eV. We performed Co L_3 -edge RIXS with the AGM-AGS spectrometer [37] at TLS beamline 05A of NSRRC. The total energy resolution of RIXS was 90 meV; the base pressure of the RIXS chamber was 1×10^{-8} torr. Samples were cooled to 20 K with liquid helium. The RIXS scattering plane was in the ac plane of the sample crystal; the incident and scattering angles were set to 20° and 90° , respectively. The electric-field vector ϵ of the incident beam was parallel or perpendicular to the scattering plane for π and σ polarizations, respectively.

Figure 2 shows the Co $L_{2,3}$ -edge XAS of $La_{1.5}Sr_{0.5}CoO_4$ and of the reference compounds: Sr_2CoO_3Cl , $EuCoO_3$ and CoO , which show spectra of HS Co^{3+} , LS Co^{3+} and HS Co^{2+} ions, respectively. Co $L_{2,3}$ -edge XAS spectra of $La_{1.5}Sr_{0.5}CoO_4$ with $\epsilon \perp c$ and $\epsilon \parallel c$ reproduce spectral features as so far reported[25]; There exist four pronounced features in the XAS of $La_{1.5}Sr_{0.5}CoO_4$. We focus on two features marked with vertical bars at 778 eV denoted $(L_3 - 3)$ and 780.5 eV denoted $(L_3 - 0.5)$ to unravel the contributions of HS Co^{2+} and LS Co^{3+} to the measured XAS. Among the XAS of reference samples, CoO has a much stronger XAS feature at $(L_3 - 3)$ than the others: the XAS feature at $(L_3 - 3)$ is derived mainly from the Co^{2+}

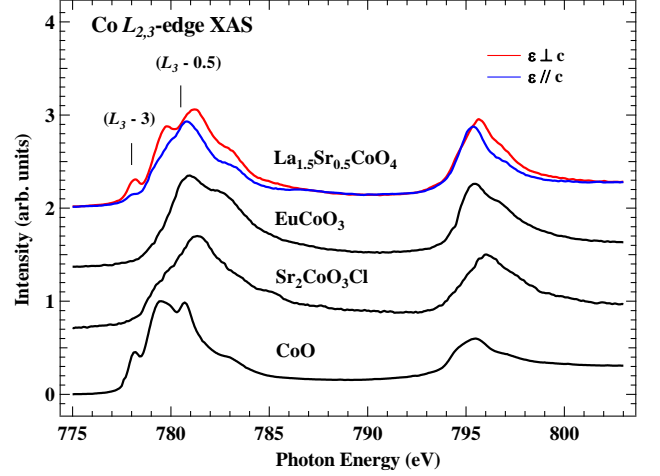


FIG. 2: Co $L_{2,3}$ -edge XAS of $La_{1.5}Sr_{0.5}CoO_4$ recorded at 25 K with $\epsilon \perp c$ and $\epsilon \parallel c$ are compared with XAS of reference Co compounds: CoO , Sr_2CoO_3Cl and $EuCoO_3$. The vertical bars indicate photon energies 778 eV and 780.5 eV denoted $(L_3 - 3)$ and $(L_3 - 0.5)$, respectively.

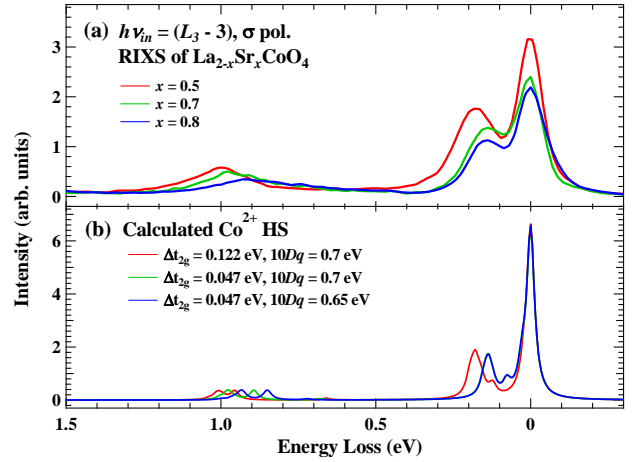


FIG. 3: Co L_3 -edge RIXS spectra of $La_{2-x}Sr_xCoO_4$ excited with σ -polarized X-rays of energy 778 eV denoted $(L_3 - 3)$. (a) RIXS spectra recorded at 20 K and normalized with the incident beam intensity. (b) Calculated RIXS spectra for HS Co^{2+} of tetragonal symmetry with various parameters of tetragonal distortion Δt_{2g} and crystal field $10Dq$.

HS state, and XAS intensity at $(L_3 - 3)$ changes linear to Co^{2+} population $(1 - x)$. In addition, all reference samples show a strong XAS intensity at $(L_3 - 0.5)$, indicating that a separation of the contributions of HS Co^{2+} , LS Co^{3+} and HS Co^{3+} states to the XAS feature of $La_{1.5}Sr_{0.5}CoO_4$ at $(L_3 - 0.5)$ is not straightforward.

To elucidate the electronic structures of Co^{2+} and Co^{3+} in $La_{1.5}Sr_{0.5}CoO_4$, we resorted to Co L_3 -edge RIXS spectral measurements. Figure 3(a) depicts Co RIXS spectra excited with σ -polarized X-rays of energy set to $(L_3 - 3)$ for samples with $x = 0.5, 0.7$ and 0.8 . In addi-

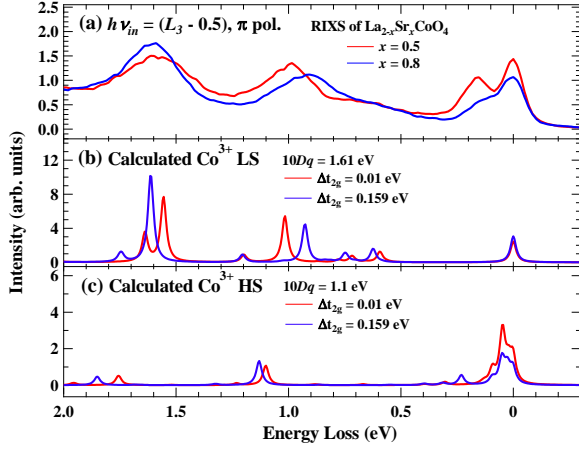


FIG. 4: (a) Measured Co L_3 -edge RIXS spectra of $\text{La}_{2-x}\text{Sr}_x\text{CoO}_4$ ($x = 0.5$ and 0.8) with incident photon energy ($L_3 - 0.5$) and π polarization. (b) & (c) Calculated RIXS spectra for LS Co^{3+} and HS Co^{3+} ions, respectively.

tion to the elastic scattering, there exist distinct RIXS features at energies about 1 eV and 0.2 eV. The former is derived from electronic transitions of Co^{2+} from the HS ground state $t_{2g}^5 e_g^2$ of symmetry ${}^4T_{1g}$ to a HS excited state $t_{2g}^4 e_g^3$ of symmetry ${}^4T_{2g}$; its excitation energy is the energy required to promote a t_{2g} electron to an e_g orbital, i.e., $10Dq$. The 0.2-eV excitation arises from transitions of Co^{2+} within the t_{2g} manifold; their excitation energies are thus affected by the tetragonal distortion but are insensitive to $10Dq$. Measurements of these RIXS excitations lead us to determine unambiguously the values of $10Dq$ and Δt_{2g} . We simulated the RIXS spectra of HS Co^{2+} with a configuration-interaction CoO_6 cluster model that includes the full atomic multiplets and the hybridization with the O $2p$ ligands [38, 39]. The calculated spectra plotted in Fig. 3(b) show two distinct excitations at energies near 0.2 eV and 1 eV, in satisfactory agreement with the RIXS measurements. The measured spectrum is best described with calculations using parameters $10Dq = 0.7$ eV and $\Delta t_{2g} = 122$ meV for HS Co^{2+} at half doping. In addition, the change of Sr doping x results in a shift of the excitations at 0.2 eV and 1 eV to lower energies in response to the change of the Co electronic structure. A comparison of these spectra with calculations shows that both the tetragonal splitting Δt_{2g} and the crystal field $10Dq$ decrease for x increasing from 0.5 to 0.8; i.e., Δt_{2g} changed from 122 meV to 47 meV and $10Dq$ from 0.7 eV to 0.65 eV. These results reveal that, for HS Co^{2+} , the tetragonal distortion of CoO_6 octahedra decreases; its in-plane Co-O bond length increases when the Sr doping x is increased.

In $\text{La}_{2-x}\text{Sr}_x\text{CoO}_4$, Co^{3+} can be in either the LS or the HS state. For large $10Dq$, the electronic configuration energetically favors the LS state, whereas the HS state is stabilized with an increased J_H , or a decreased $10Dq$.

Co L_3 -edge RIXS measurements have been demonstrated to be an effective method to probe the spin state of Co^{3+} in LaCoO_3 [21]. Here we further examined the local electronic structure of Co^{3+} in $\text{La}_{2-x}\text{Sr}_x\text{CoO}_4$, and its spin state, by tuning the incident photon energy to $(L_3 - 0.5)$. Figure 4(a) shows the RIXS spectra of $\text{La}_{2-x}\text{Sr}_x\text{CoO}_4$. We selected incident X-rays of π polarization to suppress the elastic scattering and to enhance relatively the RIXS excitations. The structures above 2 eV overlap with fluorescence. Similar to the RIXS measurements of LaCoO_3 that we reported previously [21], there exist clear but broad excitation features at 0.6 eV, 1 eV and 1.6 eV; they are spectroscopic evidence for the LS ground state of Co^{3+} . All these, in the one-electron picture, are t_{2g} -to- e_g transitions. The 1.6-eV excitation is derived from a transition of low-spin ${}^1A_{1g}$ ground state to another low-spin state of symmetry ${}^1T_{1g}$ without involving spin flips. Its excitation energy depends on the combined effect of $10Dq$, pd hybridization and the effective on-site Coulomb energy U_{dd} [21], but is less sensitive to the tetragonal distortion. The 1-eV excitation involves spin flips, resulting from transitions to the intermediate-spin (IS) ${}^3T_{2g}$ states. Its excitation energies decrease with increased tetragonal distortion.

Figures 4(b) and 4(c) show calculated RIXS spectra of LS and HS Co^{3+} ions, respectively. We used parameter values typical for Co^{3+} compounds [38]. The $10Dq$ and Δt_{2g} of LS Co^{3+} are 1.61 eV and 10 meV, respectively, for $x = 0.5$. The calculated RIXS spectra of LS Co^{3+} agree well with the measured spectra, corroborating the aforementioned symmetry explanation of excited states. In contrast, the calculated RIXS spectrum of HS Co^{3+} is dominated by elastic scattering and excitations of energy less than 0.1 eV, and fails to account for the measurements. This observation indicates that the Co^{3+} ions in the checkerboard-type charge ordering of $\text{La}_{1.5}\text{Sr}_{0.5}\text{CoO}_4$ are in the LS state, in satisfactory agreement with the results of neutron scattering [11] and XAS [25], which explain the extremely insulating nature of $\text{La}_{1.5}\text{Sr}_{0.5}\text{CoO}_4$ according to the spin-blockade mechanism.

The combined results of RIXS measurements and cluster calculations reveal that the LS Co^{3+} ion has a larger crystal-field splitting $10Dq$ than the HS Co^{2+} ion; this condition reflects the low-spin character of Co^{3+} , which leads to a much smaller ionic size and shorter Co-O bonds. In addition, both CoO_6 octahedra of HS Co^{2+} and LS Co^{3+} show a tetragonal distortion in which the apical Co-O bond is elongated along the c -axis owing to the tetragonal lattice structure [40]. The t_{2g} splitting Δt_{2g} defined in Fig. 1(b) for both cases is positive. Furthermore, the JT effect on the HS Co^{2+} modifies the t_{2g} splitting, whereas LS Co^{3+} is JT-inactive. We found that the Δt_{2g} value for HS Co^{2+} at half doping is larger than that for LS Co^{3+} ; these values are 122 meV and 10 meV, respectively.

For highly hole-doped $\text{La}_{2-x}\text{Sr}_x\text{CoO}_4$, the effective

magnetic moment per Co ion is found to be substantially decreased from $3.87 \mu_B$ at $x=0.5$ to $\approx 2.6 \mu_B$ when x is changed to 0.8, accompanied by a steep decline of the in-plane resistivity [23]. In this regime, the checkerboard charge order breaks down; there exist incommensurate charge correlations [12]. These severe changes of the magnetic and electronic properties indicate the existence of HS Co^{3+} , which might lead to incommensurate spin correlations, and a large pd hybridization.

We used RIXS to investigate also the doping dependence of the Co spin state. The intensity changes of the RIXS features shown in Fig. 4(a) provide a measure of the population changes of LS Co^{3+} and HS Co^{2+} , as plotted in Fig. 5(a). The 0.2-eV RIXS excitation arises from transitions within the t_{2g} manifold of HS Co^{2+} ; its intensity change reflects the change in the population of HS Co^{2+} . When the Sr doping x is altered from 0.5 to 0.8, the intensities of the 0.2-eV and the 1.6-eV RIXS features decrease by 48 % and increase by 20 %, respectively, revealing that the population of LS Co^{3+} increases to 60 % and that of HS Co^{2+} decreases to 20 %. In addition, the intensity of quasi-elastic scattering is decreased by only 17 %, smaller than the observed 48 % decrease in the 0.2-eV RIXS excitation, providing evidence for the existence of HS Co^{3+} in highly doped $\text{La}_{2-x}\text{Sr}_x\text{CoO}_4$. These intensity changes are summarized in Table I. From the population changes of LS Co^{3+} and HS Co^{2+} , the populations of HS Co^{3+} for $x = 0.7$ and 0.8 are estimated to be 10 % and 20 %, respectively. Our RIXS results indicate a significant population of the HS Co^{3+} state in highly Sr-doped $\text{La}_{2-x}\text{Sr}_x\text{CoO}_4$, in agreement with the evidence from XAS results [12].

Figure 5(b) shows that the $\Delta_{t_{2g}}$ splittings of HS Co^{2+} and LS Co^{3+} have opposite trends of hole-doping dependence. $\Delta_{t_{2g}}$ of LS Co^{3+} increases from 10 meV to 159 meV for x altered from 0.5 to 0.8. This significant increase in $\Delta_{t_{2g}}$ reflects the substantially decreased resistivity in the highly doped regime. As the Sr concentration is increased, there is a tendency for the doped holes of Co $3d$ to move predominantly in the ab -plane to gain band energy. The contraction in the ab -plane is consequently favorable; the tetragonal distortion is increased with increased Sr doping for LS Co^{3+} . The observed evolution of a tetragonal distortion explains the change of magnetic anisotropy from half doping to heavy doping or the limit at $x = 1$. Because the spin-orbit coupling of Co $3d$ is of the same order of magnitude as the t_{2g} splitting, a single-electron state in the partially filled t_{2g} shell can have an unquenched orbital moment. In this scheme, a t_{2g} state is better expressed in terms of a complex linear combination of $|xy\rangle$, $|yz\rangle$ and $|zx\rangle$. Wave functions denoted $|d_{\pm 1}^x\rangle$, $|d_{\pm 1}^y\rangle$ and $|d_{\pm 1}^z\rangle$ with an effective orbital momentum $\tilde{l} = 1$ can be formed for the orbital moment quantized along axes x , y and z , respectively [6, 7, 41]. At half doping, the magnetic anisotropy is dictated by

TABLE I: Ratio of integrated intensities of RIXS structures of $\text{La}_{1.2}\text{Sr}_{0.8}\text{CoO}_4$ against $\text{La}_{1.5}\text{Sr}_{0.5}\text{CoO}_4$.

	Elastic	0.2-eV	1-eV	1.6-eV
$I_{x=0.8}/I_{x=0.5}$	0.83 ± 0.05	0.52 ± 0.05	0.87 ± 0.05	1.2 ± 0.05

HS Co^{2+} , which has one hole in the t_{2g} orbitals. Because of the inherent elongation of the CoO_6 octahedron in the tetragonal lattice structure and the spin-orbit interaction, a t_{2g} hole originally in the $|xy\rangle$ orbital with no magnetic anisotropy acquires the $|d_{\pm 1}^x\rangle$ or $|d_{\pm 1}^y\rangle$ orbital character and an orbital moment in the ab -plane becomes energetically favorable [6–8]. HS Co^{2+} consequently exhibits a magnetic anisotropy in that the in-plane susceptibility χ_{ab} is larger than the out-of-plane one χ_c . In a highly doped phase in which HS Co^{2+} is largely replaced by Co^{3+} , this tendency is decreased. One can similarly argue that the HS Co^{3+} favors an elongated CoO_6 octahedron and a spin along the c -axis. There is one hole in the degenerate $|yz\rangle$ and $|zx\rangle$ orbitals, as illustrated in Fig. 1(b). If the spin-orbit interaction is included, this hole has an unquenched orbital moment in the z direction through the formation of $|d_{\pm 1}^z\rangle$, leading to an easy axis of magnetization along the c -axis. To verify the above arguments, we compared the energy change of HS Co^{3+} under an external magnetic field by using atomic multiplet calculations. The energy of HS Co^{3+} under a field of 1 T along the z -axis is lower than that without an external field by 0.21 meV; it, however, remains unchanged if the field along the x -axis. Therefore a magnetic anisotropy of $\chi_c > \chi_{ab}$ is expected in the heavily doped regime, consistent with the magnetic-susceptibility measurements of LaSrCoO_4 [42].

In summary, by tuning the resonant energy, RIXS was exploited to probe the electronic structure of transition-metal ions of specific valence in a mixed-valence compound. We obtained the crystal-field and tetragonal-distortion energies of Co^{2+} and Co^{3+} separately, and demonstrated gradual transition of Co^{3+} from the low-spin to a high-spin state with increasing Sr concentration. The crystal-field splittings $10Dq$ of LS Co^{3+} and HS Co^{2+} are 1.61 eV and 0.7 eV at half doping, respectively. The tetragonal t_{2g} splittings of HS Co^{2+} and LS Co^{3+} have opposite trends of hole-doping dependence. For the doping x altered from 0.5 to 0.8, $\Delta_{t_{2g}}$ of LS Co^{3+} increases from 10 meV to 159 meV, while that of HS Co^{2+} decreases from 122 meV to 47 meV. These results enable us also to unravel the underlying mechanism of the change of magnetic anisotropy and in-plane resistivity of $\text{La}_{2-x}\text{Sr}_x\text{CoO}_4$ through the interplay of the tetragonal distortion of the spin-orbit coupling.

We thank the NSRRC staff for technical help during our RIXS measurements at the AGM-AGS beamline of Taiwan Light Source. We thank C. F. Chang

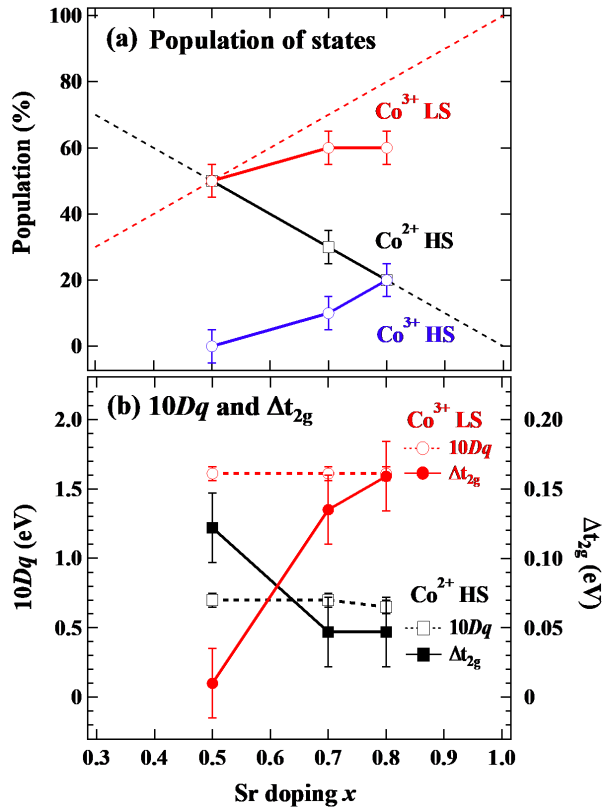


FIG. 5: Sr-doping dependence of (a) population of states estimated with RIXS results and (b) crystal field and tetragonal distortion of CoO_6 .

and A. C. Komarek for valuable discussions. This work was supported in part by the Ministry of Science and Technology of Taiwan through MOST 106-2112-M-213-008-MY3 and also by JSPS through KEKENHI No.19K03741. D. I. Khomskii was supported by the Deutsche Forschungsgemeinschaft (DFG, German Research Foundation), project number 277146847 CRC 1238.

* email: okamoto.jun@nsrrc.org.tw

† email: djhuang@nsrrc.org.tw

- [1] Y. Tokura and N. Nagaosa, *Science* **288**, 462 (2000).
- [2] M. Imada, A. Fujimori, and Y. Tokura, *Rev. Mod. Phys.* **70**, 1039 (1998).
- [3] P. Mandal, C. R. Serrao, E. Suard, V. Caignaert, B. Raveau, A. Sundaresan, and C. N. R. Rao, *J. Solid State Chem.* **197**, 408 (2013).
- [4] M. Bieringer and J. E. Greedan, *J. Solid State Chem.* **143**, 132 (1999).
- [5] T. Kimura, Y. Tomioka, A. Asamitsu, and Y. Tokura, *Phys. Rev. Lett.* **81**, 5920 (1998).
- [6] Daniel I. Khomskii, *Transition metal compounds* (Cambridge University Press, London, 2014).

- [7] N. Hollmann, M. W. Haverkort, M. Cwik, M. Benomar, M. Reuther, A. Tanaka, and T. Lorenz, *New. J. Phys.* **10**, 023018 (2008).
- [8] S. I. Csiszar, M. W. Haverkort, Z. Hu, A. Tanaka, H. H. Hsieh, H. J. Lin, C. T. Chen, T. Hibma and L. H. Tjeng, *Phys. Rev. Lett.* **95**, 187205 (2005).
- [9] B. Keimer, S. A. Kivelson, M. R. Norman, S. Uchida, and J. Zaanen, *Nature* **518**, 179 (2015).
- [10] J. G. Bednorz and K. A. Müller, *Z. Phys. B* **64**, 189(1986).
- [11] I. A. Zaliznyak, J. P. Hill, J. M. Tranquada, R. Erwin, and Y. Moritomo, *Phys. Rev. Lett.* **85**, 4353 (2000).
- [12] Z. W. Li, Y. Drees, C. Y. Kuo, H. Guo, A. Ricci, D. Lamago, O. Sobolev, U. Rütt, O. Gutowski, T. W. Pi, A. Piovano, W. Schmidt, K. Mogare, Z. Hu, L. H. Tjeng, and A. C. Komarek, *Sci. Rep.* **6**, 25117 (2016).
- [13] I. A. Zaliznyak, J. M. Tranquada, R. Erwin, and Y. Moritomo, *Phys. Rev. B* **64**, 195117 (2001).
- [14] A. T. Boothroyd, P. Babkevich, D. Prabhakaran, and P. G. Freeman, *Nature* **471**, 341 (2011).
- [15] S. M. Gaw, E. C. Andrade, M. Vojita, C. D. Frost, D. T. Adroja, D. Prabhakaran, and A. T. Boothroyd, *Phys. Rev. B* **88**, 165121 (2013).
- [16] Y. Drees, D. Lamago, A. Piovano, and A. C. Komarek, *Nat. Comm.* **4**, 2449 (2013).
- [17] Y. Drees, Z. W. Li, A. Ricci, M. Rotter, W. Schmidt, D. Lamago, O. Sobolev, U. Rütt, O. Gutowski, M. Sprung, A. Piovano, J. P. Castellan and A. C. Komarek, *Nat. Comm* **5**, 5731 (2014).
- [18] H. Guo, W. Schmidt, L. H. Tjeng, and A. C. Komarek, *Phys. Status Solidi (RRL)* **9**, 580 (2015).
- [19] Z. W. Li, Y. Drees, A. Ricci, D. Lamago, A. Piovano, M. Rotter, W. Schmidt, O. Sobolev, U. Rütt, O. Gutowski, M. Sprung, J. P. Castellan, L. H. Tjeng, and A. C. Komarek, *J. Supercond. Nov. Magn.* **29**, 727 (2016).
- [20] M. W. Haverkort, Z. Hu, J. C. Cezar, T. Burnus, H. Hartmann, M. Reuther, C. Zobel, T. Lorenz, A. Tanaka, N. B. Brookes, H. H. Hsieh, H.-J. Lin, C. T. Chen, and L. H. Tjeng, *Phys. Rev. Lett.* **97**, 176405 (2006).
- [21] K. Tomiyasu, J. Okamoto, H. Y. Huang, Z. Y. Chen, E. P. Sinaga, W. B. Wu, Y. Y. Chu, A. Singh, R.-P. Wang, F. M. F. de Groot, A. Chainani, S. Ishihara, C. T. Chen, and D. J. Huang, *Phys. Rev. Lett.* **119**, 196402 (2017).
- [22] C. I. Ballhausen, *Introduction to Ligand Field Theory* (McGraw-Hill Book Co., New York, 1962).
- [23] Y. Moritomo, K. Higashi, K. Matsuda, and A. Nakamura, *Phys. Rev. B* **55** R14725 (1997).
- [24] A. Maignan, V. Caignaert, B. Raveau, D. Khomskii, and G. Sawatzky, *Phys. Rev. Lett.* **93**, 026401 (2004).
- [25] C. F. Chang, Z. Hu, H. Wu, T. Burnus, N. Hollmann, M. Benomar, T. Lorenz, A. Tanaka, H.-J. Lin, H. H. Hsieh, C. T. Chen, and L. H. Tjeng, *Phys. Rev. Lett.* **102**, 116401 (2009).
- [26] M. Cwik, M. Benomar, T. Finger, Y. Sidis, D. Senff, M. Reuther, T. Lorenz, and M. Braden, *Phys. Rev. Lett.* **102**, 057201 (2009).
- [27] N. Sakiyama, I. A. Zaliznyak, S.-H. Lee, Y. Mitsui, and H. Yoshizawa, *Phys. Rev. B* **78**, 180406(R) (2008).
- [28] C. Tealdi, C. Ferrara, L. Malavasi, P. Mustarelli, C. Ritter, G. Chiodelli, and Y. A. Diaz-Fernandez, *Phys. Rev. B* **82**, 174118 (2010).
- [29] N. Hollmann, M. W. Haverkort, M. Benomar, M. Cwik, M. Braden, and T. Lorenz, *Phys. Rev. B* **83**, 174435

- (2011).
- [30] L. J. P. Ament, M. van Veenendaal, T. P. Devereaux, J. P. Hill, and J. van den Brink, *Rev. Mod. Phys.* **83**, 705 (2011).
 - [31] M. M. van Schooneveld, R. Kurian, A. Juhin, K. Zhou, J. Schlappa, V. N. Strocov, T. Schmitt, and F. M. F. de Groot, *J. Phys. Chem. C* **116**, 15218 (2012).
 - [32] H. Niwa, H. Takachi, J. Okamoto, W.-B. Wu, Y.-Y. Chu, A. Singh, D.-J. Huang, and Y. Moritomo, *Sci. Rep.* **7**, 16579 (2017).
 - [33] Y. Yokoyama, Y. Yamasaki, M. Taguchi, Y. Hirata, K. Takubo, J. Miyawaki, Y. Harada, D. Asakura, J. Fujioka, M. Nakamura, H. Daimon, M. Kawasaki, Y. Tokura, and H. Wadati, *Phys. Rev. Lett.* **120**, 206402 (2018).
 - [34] R.-P. Wang, A. Hariki, A. Sotonikov, F. Frati, J. Okamoto, H.-Y. Huang, A. Singh, D.-J. Huang, K. Tomiyasu, C.-H. Du, J. Kuneš, and F. M. F. de Groot, *Phys. Rev. B* **98**, 035149 (2018).
 - [35] R.-P. Wang, J. Geessinck, H. Elnaggar, Y. A. Birkhölzer, K. Tomiyasu, J. Okamoto, B. Liu, C.-H. Du, D.-J. Huang, G. Koster, and F. M. F. de Groot, *Phys. Rev. B* **100**, 165148 (2019).
 - [36] Y. Okimoto, T. Egawa, R. Fukuya, Y. Matsubara, Y. Yamada, N. Yamaya, T. Ishikawa, K. Onda, S. Koshihara, H. Taniguchi, M. Itoh, A. Isayama, and T. Sasagawa, *J. Phys. Soc. Jpn.* **82**, 074721 (2013).
 - [37] C. H. Lai, H. S. Hung, W. B. Wu, H. Y. Huang, H. W. Fu, S. W. Lin, S. W. Huang, C. C. Chiu, D. J. Wang, L. J. Huang, T. C. Tseng, S. C. Chung, C. T. Chen, and D. J. Huang, *J. Synchrotron Radiat.* **21**, 325 (2014).
 - [38] CoO₆ cluster-model calculations were performed by using Quanty (<http://www.quanty.org/>). The Slater integrals have been reduced to 70% of their atomic values. Co²⁺ parameters for $x = 0.5$ [eV]: $U_{dd} = 6.5$, $U_{cd} = 8.2$, $\Delta = 6.5$, $10Dq = 0.7$, $D_s = 0.044$, $D_t = 0.002$, $pd\sigma_{x,y} = -1.21$, $pd\sigma_z = -0.958$, $pd\pi_{x,y} = 0.615$, $pd\pi_z = 0.442$, $T_{pp} = 0.7$. Co³⁺ parameters for $x = 0.5$: $U_{dd} = 5.5$, $U_{cd} = 7.0$, $\Delta = 3.5$, $10Dq = 1.61$ for LS and 1.1 for HS, $D_s = 0.07$, $D_t = 0.04$, $pd\sigma_{x,y} = -1.37$, $pd\sigma_z = -1.16$, $pd\pi_{x,y} = 0.632$, $pd\pi_z = 0.533$, $T_{pp} = 0.7$.
 - [39] M. W. Haverkort, M. Zwierzycki, and O. K. Andersen, *Phys. Rev. B* **85**, 165113 (2012).
 - [40] M. Cwik, Ph. D. thesis, Universität zu Köln, 2007.
 - [41] $|d_{\pm 1}^x\rangle = \mp \frac{1}{\sqrt{2}}(|xy\rangle \pm i|zx\rangle)$, $|d_{\pm 1}^y\rangle = \mp \frac{1}{\sqrt{2}}(|yz\rangle \pm i|xy\rangle)$ and $|d_{\pm 1}^z\rangle = \mp \frac{1}{\sqrt{2}}(|zx\rangle \pm i|yz\rangle)$
 - [42] H. Guo, Z. Hu, T.-W. Pi, L. H. Tjeng, and A. C. Komarek, *Crystals*, **6**, 98 (2016).